Materials Advances

ROYAL SOCIETY OF CHEMISTRY

PAPER

View Article Online
View Journal | View Issue

Cite this: *Mater. Adv.*, 2024, 5, 259

White light-activated bactericidal coating using acrylic latex, crystal violet, and zinc oxide nanoparticles

Gi Byoung Hwang, †[a] Joe Stent,†[a] Sacha Noimark, [a] Ki Joon Heo, [b] Alexander J. MacRobert,[c] Christopher W. M. Kay, [de] Enrico Salvadori, [f] Charlotte K. Williams, [g] Sebastian D. Pike, [h] Milo S. P. Shaffer, [i] Elaine Allan[j] and Ivan P. Parkin *[a]

In this study, a white light-activated bactericidal coating consisting of acrylic latex, zinc oxide nanoparticles (ZnO NPs) and crystal violet (CV) was produced through a two-step dipping process. CV molecules and ZnO NPs were incorporated into an acrylic latex coating deposited onto a glass substrate. After the incorporation, the colour of the coating surface changed to purple from colourless and XPS sputtering analysis showed the existence of ZnO NPs within the coating. In a bactericidal test, the CV dyed samples showed an intrinsic bactericidal activity (0.7–0.88 log reduction in viable bacteria number) against *S. aureus* whereas it was not observed on *E. coli* in the dark. Upon white light irradiation (light intensity: 512 lux), the bactericidal activity of the CV-dyed sample was significantly enhanced. Compared to the control, the CV-dyed samples showed 1.16–2.51 log reduction against both bacterial strains in white light. In terms of the testing against *S. aureus* in white light, ZnO NPs addition into the CV-dyed sample showed enhanced bactericidal activity. The bactericidal activity of the CV-dyed sample with ZnO NPs was 1.34 log higher than the CV-dyed sample. Based on data obtained from TR-EPR spectroscopy, it is speculated that the addition of ZnO NPs into the dye induces an alternative photoredox pathway, resulting in more generation of reactive oxygen species lethal to bacterial cells. It is expected that this technique could be used to transform a wide range of surfaces into bactericidal surfaces and contribute to maintaining low pathogen levels on hospital surfaces related to healthcare-associated infection.

Received 5th August 2023,
Accepted 12th October 2023

DOI: 10.1039/d3ma00509g

rsc.li/materials-advances

1. Introduction

With the rise of bacterial drug resistance, there is an urgent need to decrease the spread of bacteria in healthcare environments and reduce the risk of hospital-associated infections (HAIs). HAIs cause symptoms ranging from minor patient discomfort to prolonged or permanent disability and even, in some cases, death.[1,2] In England, there are at least 300 000 HAIs annually resulting in 5000 patient deaths.[3] Contaminated surfaces contribute to pathogen transmission in hospitals *via* contact with both patients and healthcare personnel.[4–6] It was reported that 70% of HAIs are associated with bacterial contamination of hospital surfaces or medical devices.[7–9] Vigorous hospital cleaning routines have been implemented and have impacted the levels of surface contamination.[6,10] However, it is difficult to maintain clean surfaces in hospitals and even small numbers of residual bacteria can rapidly reproduce if conditions are favourable, resulting once again in high levels of surface contaminants.

[a] *Department of Chemistry, University College London, 20 Gordon Street, London, WC1H 0AJ, UK. E-mail: i.p.parkin@ucl.ac.uk; Tel: +44(0)207 679 4669*
[b] *School of Mechanical Engineering, Chonnam National University, Gwangju, 61186, Republic of Korea*
[c] *UCL Division of Surgery and Interventional Science, UCL medical School, Rowland Hill Street, London, NW3 2PF, UK*
[d] *London Centre for Nanotechnology, University College London, 17-19 Gordon Street, London, WC1H 0AH, UK*
[e] *Department of Chemistry, Saarland University, Saarbrücken 66123, Germany*
[f] *Department of Chemistry and NIS Centre, University of Torino, Via Pietro Giuria 7, 10125 Torino, Italy*
[g] *Department of Chemistry, Chemistry Research Laboratory, University of Oxford, Oxford, OX13TA, UK*
[h] *Department of Chemistry, University of Warwick, Coventry, CV4 7SH, UK*
[i] *Departments of Chemistry & Materials, Imperial College London, South Kensington, London, SW7 2AZ, UK*
[j] *Department of Microbial Diseases, UCL Eastman Dental Institute, London, NW3 2PF, UK*
† Equivalently contributed.

One promising strategy to reduce bacterial surface contamination in healthcare environments is the use of light-activated bactericidal surfaces. Significant research has focused on the use of titanium dioxide nanoparticles (TiO_2 NPs), which effectively kill bacteria under ultraviolet (UV) irradiation.[11–14] UV irradiation of TiO_2 NPs results in the generation of reactive oxygen species (ROS) containing hydroxyl radicals ($^{\bullet}OH$) and singlet oxygen ($^1O_2$). The ROS initiate a multi-site attack against bacteria resulting in loss of membrane integrity, inactivation of enzymes, and DNA damage, causing cell death.[14] However, since TiO_2 NPs are UV-activated photocatalysts, they exhibit poor bactericidal activity in white light which is widely used in hospitals.[14–16] In recent years, to overcome this shortcoming, research has focused on enhancing the photocatalytic activity of TiO_2 in white light.[17–19] It was reported that doping silver or vanadium into TiO_2 enhanced light-activated bactericidal activity in white light.[19,20] Zinc oxide (ZnO) is also a widely used inorganic photocatalyst. ZnO is considered a more efficient photocatalyst than TiO_2 because it is activated under both UV and white light.[21–23] ZnO has been shown to generate significant ROS concentrations even in white light, particularly in a wavelength range of 400–500 nm.[24]

Crystal violet (CV) and methylene blue (MB) are photosensitiser dyes which mainly absorb visible light and demonstrate light-activated bactericidal activity.[25,26] Irradiation of these dyes results in ROS generation.[27,28] Recent research showed the incorporation of photosensitiser dyes into polymer materials for use in hospital surfaces or medical devices such as tracheal and urinary catheters to decrease bacterial surface contamination.[25–30] Medical grade silicone and polyurethane were incorporated with the dyes using a simple swell–encapsulation–shrink process and the resultant dye-incorporated materials exhibit light-activated bactericidal activity in white light.[25,26,29] The additional incorporation of gold (Au) NPs or ZnO NPs into the dye-treated polymers significantly enhanced the light-activated bactericidal activity and these materials also demonstrated significant bactericidal activity in the dark.[26,31–33]

In this study, we present a simple technique for developing a white light-activated bactericidal coating (WLABC). CV and ZnO NPs incorporated acrylic latex was coated onto glass slides. WLABC was characterised using UV-vis spectroscopy and a water contact angle meter and the photo and water stabilities of the coating were tested. Bactericidal tests against *Staphylococcus aureus* (*S. aureus*) and *Escherichia coli* (*E. coli*) showed that WLABC had limited bactericidal activity in the dark, but it is significantly enhanced in white light with an intensity of 512 lux.

2. Experimental section

Solution A

80 mL of acrylic latex (X935-33, AzkoNovel, Amsterdam, Netherlands) was mixed with 20 mL of toluene (Fisher Scientific, England, UK).

Solution B

Di(octyl) phosphinic acid (DOPA)-capped ZnO NPs (~5 nm) were prepared *via* previously described methods.[23,34,35] ZnO NPs were gently heated to disperse in toluene (3 mg mL^{-1}) and subsequently mixed with acrylic latex (1 : 4 ZnO NPs/toluene : acrylic latex).

Solution C

CV solution (5 mM) was prepared using deionised (DI) water.

2.1. White light-activated bactericidal coating

As shown in Fig. 1, WLABC was prepared using a dip-coating method.

Control. Glass slide (76 mm × 26 mm) was immersed in solution A to a depth of 4 cm and withdrawn at a speed of 120 cm min^{-1}. The samples were subsequently air-dried for 24 h, washed using DI water and further air-dried for 24 h.

Sample with ZnO NPs. Glass slide was immersed in solution B to a depth of 4 cm and withdrawn at a speed of 120 cm min^{-1}. The samples were subsequently air-dried for 24 h, washed using DI water and further air-dried for 24 h.

CV-dyed sample. Control was immersed in 50 mL of solution C for 24 h and it was air-dried for 24 h in a dark room. The sample was washed using DI water and further air-dried for 24 h in a dark room.

CV-dyed sample with ZnO NPs. The sample with ZnO NPs was dipped into 50 mL of solution C for 24 h. After that, it was washed using DI water and dried for 24 h. After drying, the sample was washed using DI water and further dried for 24 h.

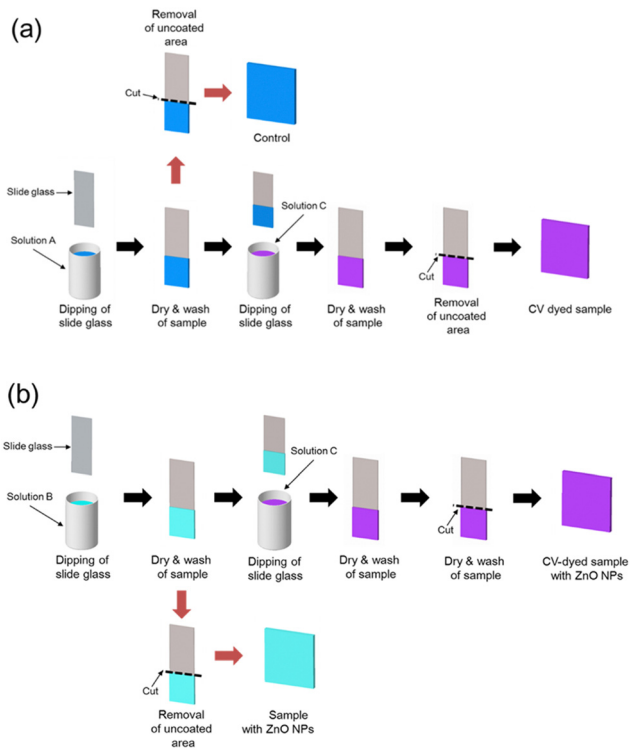

Fig. 1 Preparation of (a) control, CV-dyed sample, (b) sample with ZnO NPs, and CV-dyed sample with ZnO NPs. Solution A is a mixture of acrylic latex and toluene, solution B is a mixture of ZnO NPs and acrylic latex and solution C is crystal violet solution.

After sample preparation, the uncoated area was removed using a glass cutter.

2.2. Characterisation

UV-vis absorption spectra of the coated samples were measured in a wavelength range of 250–1000 nm using a PerkinElmer Lambda 25 spectrometer. To determine ZnO NPs encapsulation within the samples, X-ray photoelectron spectroscopy (XPS) was carried out on a Thermo K-Alpha spectrometer using monochromated Al Kα radiation. The sample with ZnO NPs and CV-dyed sample with ZnO NPs were analysed and data were collected in a binding energy of 0–1200 eV. The data for all samples were calibrated to adventitious carbon at 284.8 eV.

A static water contact angle was measured for all samples. A droplet (~5 μL) of DI water was inoculated onto the sample surface, the samples were photographed side on, and the images were analysed using FTA32 software.

2.3. Stability test

To determine the photostability of CV in samples, both the CV-dyed sample and CV-dyed sample with ZnO were exposed to white light with an intensity of ~5489 lux for 1080 h. At regular time intervals, the absorbance change of the samples at 590 nm was determined spectroscopically.

The CV stability within the CV-dyed sample and CV-dyed sample with ZnO NPs was tested when they were exposed to water. The samples were immersed in 40 mL of phosphate-buffered saline (PBS) for 3000 h. At periodic time intervals, PBS was taken and then measured at 590 nm using a UV-vis spectrometer to measure CV molecules leached from the sample to PBS. The CV concentration was calculated using the Beer–Lambert law as below.

$$c = A/(\varepsilon \times b)$$

where c is the concentration of crystal violet, A is an absorbance at 590 nm, ε is a molar extinction coefficient for crystal violet in water at 590 nm of 87 000 M^{-1} cm^{-1}, and b is the path length of the cuvette (1 cm).[36]

2.4. Bactericidal testing

In bactericidal testing, *E. coli* (ATCC 25922) and *S. aureus* (NCTC 13143) were used. The bacteria were stored at −70 °C in brain-heart-infusion broth (BHI broth, Oxoid Ltd, Hampshire, England, UK) containing 20% (v/v) glycerol and propagated on either MacConkey agar (Oxoid Ltd) in the case of *E. coli* or mannitol salt agar (Oxoid Ltd) in the case of *S. aureus*. BHI broth (10 mL) was inoculated with one colony and cultured at 37 °C for 18 h with shaking at 200 rpm. The bacteria were harvested by centrifugation (21 °C, 4000 rpm for 8 min), washed using 10 mL of PBS, and centrifuged again to recover the bacteria which were re-suspended in 10 mL of PBS. The bacterial suspension was diluted 1000-fold to obtain the inoculum with ~10^6 CFU mL^{-1}. 25 μL of bacterial suspension was inoculated onto the samples and covered with a sterile coverslip (2.2 cm × 2.2 cm) to ensure good contact between the bacteria and the sample surface. Subsequently, the samples were placed in Petri dishes with moistened filter paper to maintain humidity and exposed to white light (512 lux) whilst an identical set of samples was maintained in the dark. After the light irradiation, the samples were placed in 10 mL of PBS and vortexed for 30 s. The washed suspension was concentrated into 150 μL by centrifugation (21 °C, 4000 rpm for 8 min), serially diluted, plated on agar and then incubated at 37 °C for 24 h (*E. coli*) and 48 h (*S. aureus*). The colonies that grew on the plates were counted.

2.5. Time resolved-electron paramagnetic resonance (TR-EPR) spectroscopy

A Bruker E580 pulsed EPR spectrometer, operating at X-band frequencies (9–10 GHz/0.3 T) was used to record the TR-EPR spectra of the CV and CVZnO samples (1.5 cm × 2 cm) under aerobic conditions. The sample was irradiated with a pulsed laser excitation (~10 mJ per pulse) at a wavelength of ~660 nm. An Oxford Instruments CF935 flow cryostat was used to cool the sample using liquid helium and the temperature was maintained (50 K) using an Oxford Instruments ITC 503 temperature controller.

2.6. Statistical analysis

T-tests on experimental data were calculated using a statistical function of Microsoft Excel, version 2308.

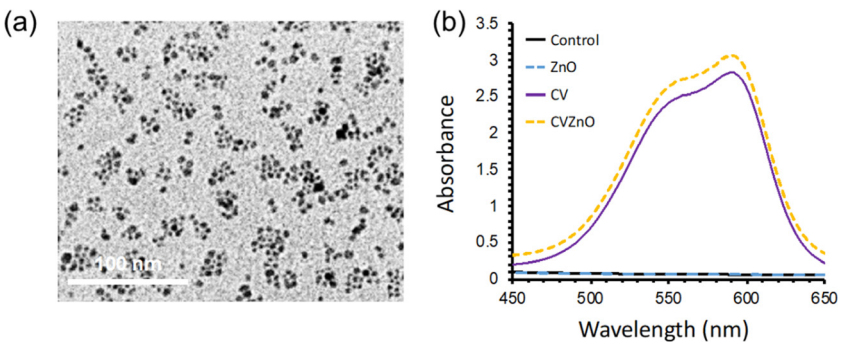

Fig. 2 (a) TEM image of ZnO NPs and (b) UV-vis absorption spectra of control, sample with ZnO NPs (ZnO), CV-dyed sample (CV), and CV-dyed sample with ZnO NPs (CVZnO) in a wavelength of 450–650 nm.

3. Results and discussion

To characterise ZnO NPs, transmission electron microscopy (TEM) measurements were carried out (Fig. 2(a)). The TEM image showed that the size of ZnO NPs was ~5 nm. UV-vis absorbance spectra of the samples were measured over a wavelength range of 250–1000 nm. As shown in Fig. 2(b), the CV-dyed sample had a main absorption at 590 nm, with a shoulder peak at 550 nm. The CV-dyed sample with ZnO NPs showed a slight increase in optical absorption, compared with the CV-dyed sample.

CV-dyed samples with ZnO NPs and samples with ZnO NPs were analysed using XPS to determine the presence of ZnO NPs within the top 1–12 nm of the sample surface. As shown in Fig. 3, XPS shows the presence of ZnO NPs at the sample surface and within the polymer bulk. A doublet peak at a binding energy of 1044 and 1021 eV corresponds to Zn $2p_{1/2}$ and $2p_{3/2}$ indicating ZnO NPs.

The surface wettabilities of the control, sample with ZnO NPs, CV-dyed sample and CV-dyed sample with ZnO NPs were measured using a water contact angle meter. As shown in Table 1, all samples gave water contact angles of $<90^{\circ}$ indicating hydrophilicity. The addition of CV or ZnO NPs into the acrylic latex-coated samples slightly increased the water contact angle.

The bactericidal activity of the control, CV-dyed sample, sample with ZnO NPs and CV-dyed sample with ZnO NPs was tested against *E. coli* and *S. aureus* in the dark and in white light. Fig. 4 shows the bactericidal activity of the control and treated samples against *S. aureus* in the dark and in white light. The light intensity of the used white lamp was 512 ± 51 lux. In the dark, the sample with ZnO NPs did not show bactericidal activity against *S. aureus* compared to the control (*P*-value >0.05) while the CV-dyed sample and CV-dyed sample with ZnO NPs demonstrated limited bactericidal activity with 0.7 and 0.88 log reductions in the number of viable bacteria, respectively (*P*-value <0.01). Upon 3 h irradiation of the white light, a 0.33 log reduction in bacterial numbers was observed on the sample with ZnO NPs alone, compared to the control (*P*-value <0.05). Bactericidal enhancement was observed on CV-dyed samples after 3 h exposure to white light and the CV-dyed sample with ZnO NPs demonstrated the most potent bactericidal activity (*P*-value <0.01). Compared to the control, a 1.16 and 2.51 log reduction in the number of viable bacteria was observed on the CV-dyed sample and the CV-dyed sample with ZnO NPs, respectively after 3 h exposure to white light.

Table 1 Static water contact angle of control, sample with ZnO NPs (ZnO), CV-dyed sample (CV) and CV-dyed sample with ZnO NPs (CVZnO)

Sample	Water contact angle (°)
Control	24.7 ± 2.0[a]
ZnO	50.2 ± 2.4
CV	69.0 ± 1.6
CVZnO	62.7 ± 4.5

[a] Average water contact angle ± standard deviation.

Fig. 5 shows the bactericidal activity of the samples against *E. coli* under dark and under white light conditions. After 4 h incubation in the dark, a statistically significant reduction in the number of bacteria was not observed for all the samples as expected (*P*-value >0.05). After 4 h exposure to white light, all treated samples showed enhanced bactericidal activity compared to the same materials in the dark. Compared to the control, a 1.55 log reduction in bacterial numbers was observed on the sample containing ZnO NPs alone and ~2.0 log reduction in bacterial numbers was observed on both the

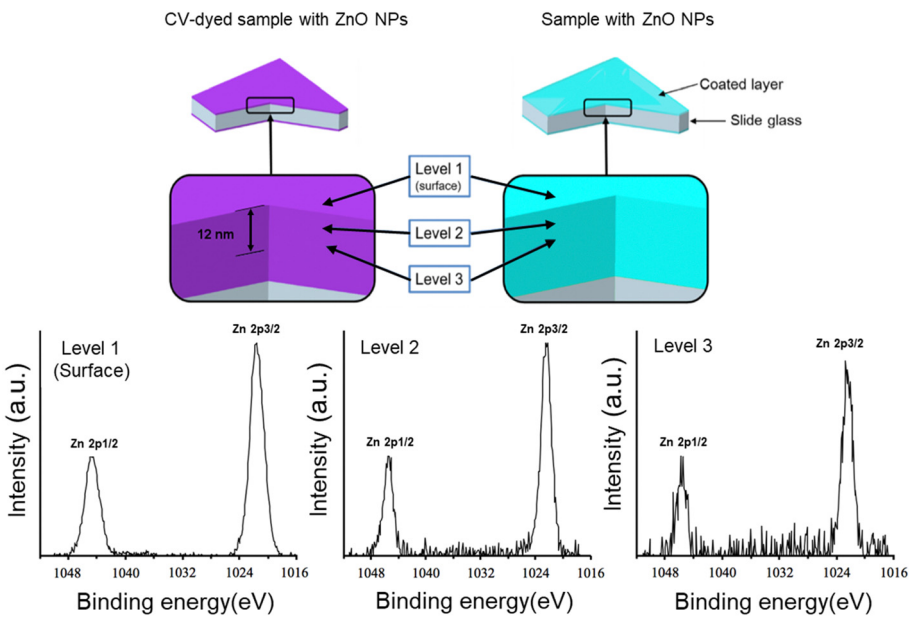

Fig. 3 XPS spectra of sample with ZnO NPs and CV-dyed sample with ZnO NPs. The presence of ZnO NPs on the surface of the samples or encapsulated within the samples was investigated with a sputtering time of 30 s per level.

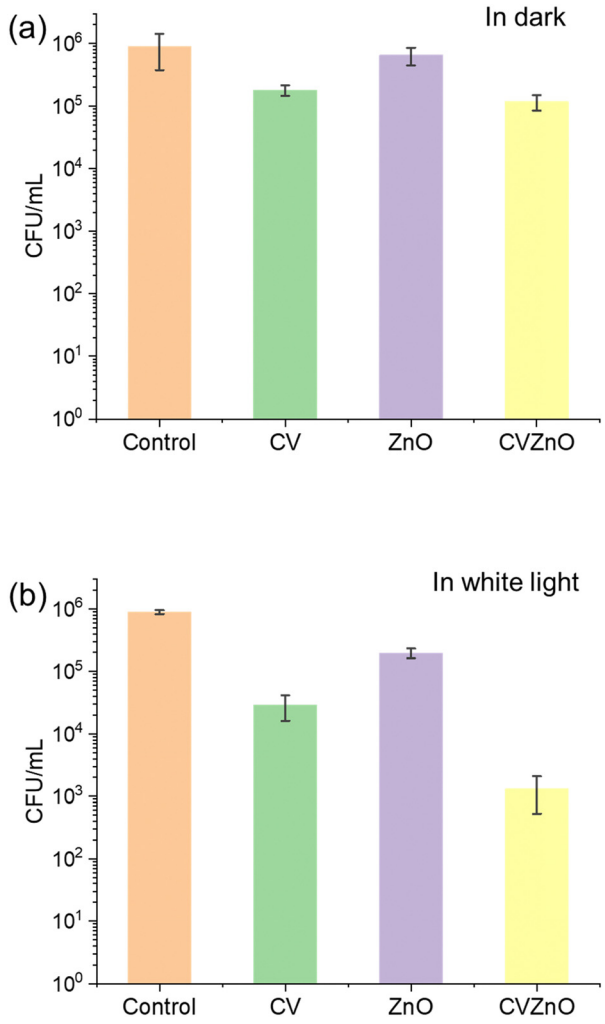

Fig. 4 Bactericidal activities of control, CV-dyed sample (CV), sample with ZnO NPs (ZnO), and CV-dyed sample with ZnO NPs (CVZnO) against *S. aureus* in (a) dark and in (b) white light. The samples were exposed to white light source with an intensity of 512 lux for 3 h and another set was incubated for 3 h in dark room. All experiments were performed at 20 °C.

CV-dyed sample and the CV-dyed sample containing ZnO NPs (*P*-value <0.01).

It is interesting to note that the incorporation of ZnO NPs into CV-dyed samples significantly enhanced the light-activated bactericidal activity against *S. aureus* compared to the material containing CV alone (*P*-value <0.01), but no such increase was observed for *E. coli* (*P*-value >0.05). This is presumably the result of the barrier function of the Gram-negative outer membrane which impedes the passage of ROS.[32]

The bactericidal mechanism of crystal violet can be explained as follow: upon white light irradiation, crystal violet molecules are excited from a ground state, and the molecule is transformed to a long-lived triplet state *via* a short-lived higher lying singlet excited state. The molecules in the triplet state undergo two photoreaction pathways including redox reactions related to the generation of superoxide radical (O_2^-), hydrogen peroxide (H_2O_2), $^\bullet$OH, and quenching by oxygen molecules related to $^1O_2$ generation. The reactive oxygen species initiate a multisite attack on bacteria, causing bacterial cell death.[37,38]

To understand the mechanism of the bactericidal activity enhanced by ZnO NPs, a change in the triplet state of the crystal violet was determined using TR-EPR spectroscopy in CV-dyed samples, with and without ZnO NPs addition into the coating. TR-EPR spectroscopy can be used to substantiate a triplet state formation in the materials and gain further information on the properties of the photo-excited triplet state.[39] The TR-EPR spectra for the samples were simulated using the EasySpin toolbox on MATLAB™ and compared to data obtained from the spectroscopy. The relative populations of the three triplet sublevels, $p_x:p_y:p_z$ was calculated to be 0 : 0.45 : 0.55, respectively, whereas the zero-field splitting parameters, D and E, which describe the magnetic dipolar interactions between the two unpaired electrons, were determined to be $|D|$ = 1650 MHz and $|E|$ = 315 MHz, in line with a previous literature report.[40] An isotropic g value (equal to free electron g value) where $g_x:g_y:g_z$ = 2.003 was used in the simulations. The spectra indicate the presence of spin-polarised triplet states of organic aromatic molecules, which are non-Boltzmann populated. These values indicate that the triplet states are localised on the crystal violet in both CV-dyed samples Fig. 6(a). It was confirmed that the profile line of the two spectra was similar, but their intensity was different, indicating the addition of ZnO NPs to the sample does not cause rearrangement in the populations within the triplet state. Previous studies with MB and 2 nm Au NPs encapsulated in silicone also demonstrated no significant change in line profile, indicating no alteration in the excited state populations.[33] However, the addition of ZnO NPs into the CV-dyed sample decreased the intensity of the EPR spectrum (Fig. 6(b)). Based on MATLAB™ simulations, it was estimated that there was a 40% decrease in the production of the triplet state. Previous studies showed that it produced an alternative pathway for photoexcited electrons when semiconductive materials were added into crystal violet indicating that the material acts as an electron acceptor, inducing the generation of reactive oxygen species.[41,42] Thus, it is speculated that instead of changing into a triplet state, the photoexcited electrons in crystal violet flowed into ZnO NPs and it induced more reactive oxygen species than the CV sample. As a result, the population in the triplet state became lower after the addition of ZnO NPs.

Previous studies showed that the addition of 1.3 nm gold nanoclusters ($[Au_{25}(Cys)_{18}]$) into CV-treated polymer showed bactericidal activity at a light intensity of ~300 lux and promoted the generation of H_2O_2 only.[42] Our research showed that 5 nm ZnO NPs addition to the dye showed photobactericidal activity at a slightly higher intensity than that of $[Au_{25}(Cys)_{18}]$. However, it was reported that the ZnO NPs addition to the dye enhanced the generation of $^1O_2$ and H_2O_2 in white light and smaller nanoparticles doping more efficiently enhanced photocatalytic reaction.[30,43,44] Thus, adding ~1 nm ZnO NPs to crystal violet is expected to improve photobactericidal activity at white light flux levels of <500 lux and to facilitate more ROS multisite attacks on bacteria than that of the combination of $[Au_{25}(Cys)_{18}]$ and CV.

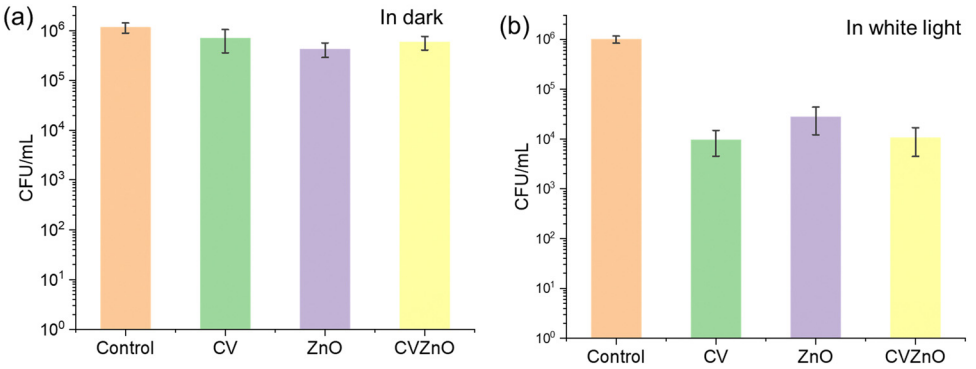

Fig. 5 Bactericidal activities of control, CV-dyed sample (CV), sample with ZnO NPs (ZnO), and CV-dyed sample with ZnO NPs (CVZnO) against *E. coli* in (a) dark and in (b) white light. The samples were exposed to white light source with an intensity of 512 lux for 4 h and another set was incubated for 4 h in dark room. All experiments were performed at 20 °C.

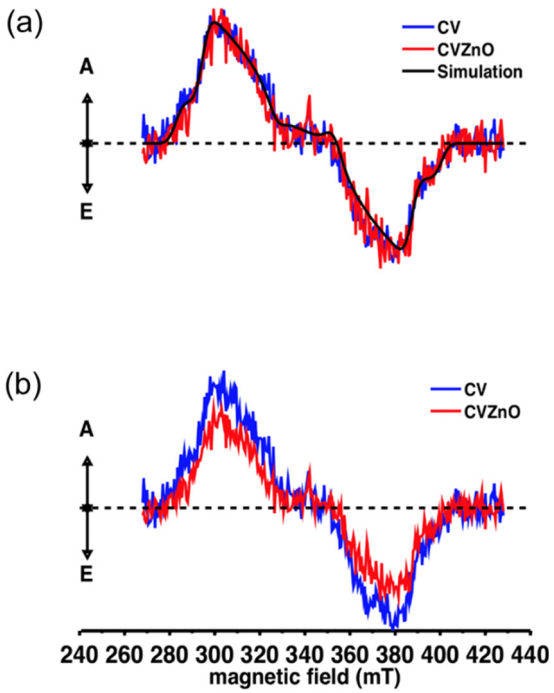

Fig. 6 Time-resolved electron plasmon resonance spectra of CV and CVZnO (a) normalised spectra and relative MATLAB simulation superimposed and (b) non-normalised primary data.

The photostability of the CV-dyed sample and the CV-dyed sample with ZnO NPs under white light with an intensity of 5489 lux was monitored using UV-vis spectroscopy. The samples were irradiated for 1080 h and the absorbance at 590 nm was measured at regular intervals to determine degradation of the dye. As shown in Fig. 7, CV intensities of the CV-dyed sample and CV-dyed sample with ZnO NPs decreased by 62% and 73% over 1080 h, respectively. The light intensity used in this study is 20 times higher than white light which is commonly found in hospital corridors and wards.[31] It is anticipated that the photodegradation of the CV dye will be much slower in a healthcare setting as degradation is a function of light intensity.

To determine CV stability within the coating, CV-dyed samples were immersed in 40 mL of PBS solution and observed for 3000 h. The CV release from CV-dyed samples into PBS was determined at 590 nm using UV-vis spectroscopy. As shown in Fig. 8, CV molecules were partially released from the coating samples into PBS for 3000 min and any further leaching was not observed. The CV concentration in PBS was <580 nM. According to previous studies, CV at a concentration of <1000 nM does not show intrinsic bactericidal activity; it also demonstrates limited or no light-activated bactericidal activities.[45] Considering the concentration of used CV (~ 5 mM) to produce bactericidal coating, the total amount of CV leaching was negligible ($<1\%$ of the total).

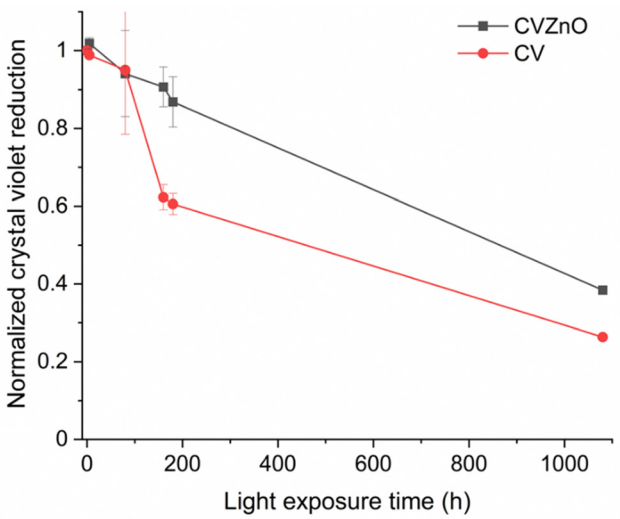

Fig. 7 Photodegradation of CV-dyed sample (CV) and CV-dyed sample with ZnO NP (CVZnO) under white light irradiation for 1080 h. The samples were exposed to white light source with a light intensity of 5489 lux. The absorbance of samples was periodically measured at 590 nm using a UV-Vis spectrometer. Normalized crystal violet reduction = optical density time at 550 nm/optical density control, standard at 550 nm; optical density time represents optical density of sample at white exposure time *t*, and optical density control, standard is optical density of samples before white light exposure.

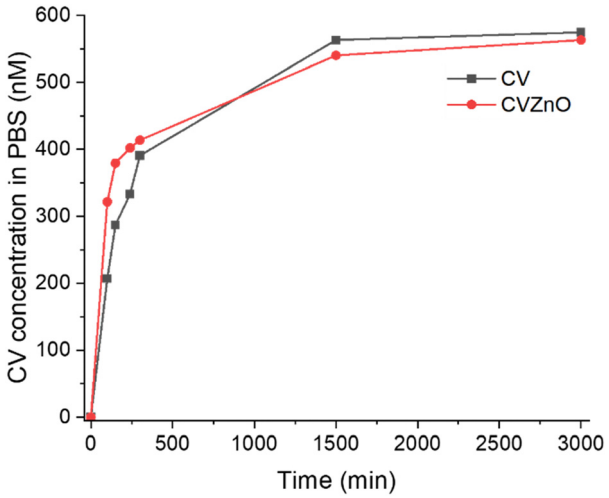

Fig. 8 CV leaching from CV-dyed sample and CV-dyed sample with ZnO NPs into PBS. The samples were immersed in 40 mL of PBS solution for 3000 min.

4. Conclusion

In this study, a white light-activated bactericidal coating using acrylic latex, zinc oxide nanoparticles (ZnO NPs) and crystal violet (CV) was produced. Through a simple dipping process, a glass slide was coated with acrylic latex, CV and ZnO NPs. In bactericidal tests against *S. aureus* and *E. coli* in the dark, the CV-dyed sample, the sample with ZnO NPs alone and the CV-dyed sample containing ZnO NPs showed some intrinsic bactericidal activity with 0.21–0.88 log reduction in bacterial numbers. In the light, the CV-dyed sample and the CV-dyed sample containing ZnO NPs showed an enhanced bactericidal activity compared to the same materials in the dark. In white light (intensity: 517 lux), the reductions in the number of viable bacteria on the CV-dyed sample and CV-dyed sample with ZnO NPs against *S. aureus* and *E. coli* were 1.16–2.01 and 1.97–2.51 log reduction after 3 and 4 h exposure to white light, respectively. A bactericidal activity of the CV-dyed sample enhanced by ZnO NPs was observed when tested against *S. aureus* in white light. The bactericidal activity of the CV-dyed sample with ZnO NPs was 1.34 log higher than the CV-dyed sample. TR-EPR spectroscopy showed that the additional incorporation of ZnO NPs within CV-dyed samples decreased the population of molecules in the triplet state. It is speculated that adding ZnO NPs into the dye produces an alternative pathway for excited electrons, inducing more reactive oxygen species lethal to bacterial cells. The acrylic latex employed in this research is a copolymer of vinyl acetate and butyl acrylate, and it is commonly used as a house paint component.[37] Because of its superior wet adhesion, it can be applied to wood, stucco and metal surfaces. Thus, it is expected that this technique can be applied to a wide range of surfaces in hospitals to potentially reduce hospital-associated infections.

Conflicts of interest

There are no conflicts to declare.

Acknowledgements

E. S. acknowledges support through Project CH4.0 under the MUR program "Dipartimenti di Eccellenza 2023-2027" (CUP: D13C22003520001). S. D. P. thanks the EPSRC for financial support (EP/K035274/1 and EP/M013839/1). S. N. thanks EPSRC UKRI Innovation Fellowship (EP/S001506/1) for financial support.

References

1 Committe of public account, Report 2004/05 improving patient care by reducing the risks of hospital acquired infection: a progress report House of Commons, The Stationery Office, 2005.
2 L. Avery, R. Bennett, K. Brinsley-Rainisch, M. Boyter, N. Coffin, S. Deshpande, M. A. Dudeck, J. R. Edwards, S. Fuller, R. Maciejewski, P. J. Malpiedi, F. Maxineau, L. C. McDonald, R. Pecoraro, K. D. Peterson, M. M. Soe, J. Snow, A. Tumpey, L. M. Weiner, J. Young and K. Zimmerman, National and state healthcare associated infections progress report, 2015, Centers for disease control and prevention (CDC), 2015.
3 Committe of public account, Reducing healthcare associated infection in hospitals in England, House of commons, The stationery office.
4 G. A. J. Ayliffe, B. J. Collins, E. J. L. Lowbury, J. R. Babb and H. A. Lilly, *J. Hyg.*, 1967, **65**, 515–536.
5 K. Page, M. Wilson and I. P. Parkin, *J. Mater. Chem.*, 2009, **19**, 3819–3831.
6 J. M. Boyce, *J. Hosp. Infect.*, 2007, **65**, 50–54.
7 P. Castelli, R. Caronno, S. Ferrarese, V. Mantovani, G. Piffaretti, M. Tozzi, C. Lomazzi, N. Rivolta and A. Sala, *Surg. Infect.*, 2006, **7**(suppl 2), S45–S47.
8 J. D. Bryers and B. D. Ratner, *BMC Oral Health*, 2006, **6**(suppl 1), S15.
9 M. Haque, M. Sartelli, J. McKimm and M. Abu Bakar, *Infect. Drug Resist.*, 2018, **11**, 2321–2333.
10 K. Page, M. Wilson, N. J. Mordan, W. Chrzanowski, J. Knowles and I. P. Parkin, *J. Mater. Sci.*, 2011, **46**, 6355–6363.
11 L. Zhao, P. K. Chu, Y. Zhang and Z. Wu, *J. Biomed. Mater. Res.*, 2009, **91**, 470–480.
12 W. A. Daoud, J. H. Xin and Y.-H. Zhang, *Surf. Sci.*, 2005, **599**, 69–75.
13 L. Visai, L. De Nardo, C. Punta, L. Melone, A. Cigada, M. Imbriani and C. R. Arciola, *Int. J. Artif. Organs*, 2011, **34**, 929–946.
14 H. A. Foster, I. B. Ditta, S. Varghese and A. Steele, *Appl. Microbiol. Biotechnol.*, 2011, **90**, 1847–1868.
15 A. Fujishima, T. N. Rao and D. A. Tryk, *J. Photochem. Photobiol., C*, 2000, **1**, 1–21.
16 A. M. Alotaibi, P. Promdet, G. B. Hwang, J. Li, S. P. Nair, S. Sathasivam, A. Kafizas, C. J. Carmalt and I. P. Parkin, *ACS Appl. Mater. Interfaces*, 2021, **13**, 10480–10489.
17 L. Zhang, J. C. Yu, H. Y. Yip, Q. Li, K. W. Kwong, A.-W. Xu and P. K. Wong, *Langmuir*, 2003, **19**, 10372–10380.

18 K. Sunada, T. Watanabe and K. Hashimoto, *Environ. Sci. Technol.*, 2003, **37**, 4785–4789.
19 E. Stathatos, P. Lianos, P. Falaras and A. Siokou, *Langmuir*, 2000, **16**, 2398–2400.
20 M. R. Elahifard, S. Rahimnejad, S. Haghighi and M. R. Gholami, *J. Am. Chem. Soc.*, 2007, **129**, 9552–9553.
21 Y. Li, W. Zhang, J. Niu and Y. Chen, *ACS Nano*, 2012, **6**, 5164–5173.
22 S. Baruah, M. Jaisai, R. Imani, M. M. Nazhad and J. Dutta, *Sci. Technol. Adv. Mater.*, 2010, **11**, 055002.
23 S. K. Sehmi, S. Noimark, S. D. Pike, J. C. Bear, W. J. Peveler, C. K. Williams, M. S. Shaffer, E. Allan, I. P. Parkin and A. J. MacRobert, *ACS Omega*, 2016, **1**, 334–343.
24 A. Lipovsky, Z. Tzitrinovich, H. Friedmann, G. Applerot, A. Gedanken and R. Lubart, *J. Phys. Chem. C*, 2009, **113**, 15997–16001.
25 E. Ozkan, E. Allan and I. P. Parkin, *RSC Adv.*, 2014, **4**, 51711–51715.
26 S. Noimark, J. Weiner, N. Noor, E. Allan, C. K. Williams, M. S. P. Shaffer and I. P. Parkin, *Adv. Funct. Mater.*, 2015, **25**, 1367–1373.
27 M. Wainwright, *J. Antimicrob. Chemother.*, 1998, **42**, 13–28.
28 M. R. Hamblin and T. Hasan, *Photochem. Photobiol. Sci.*, 2004, **3**, 436–450.
29 S. Perni, C. Piccirillo, J. Pratten, P. Prokopovich, W. Chrzanowski, I. P. Parkin and M. Wilson, *Biomaterials*, 2009, **30**, 89–93.
30 S. K. Sehmi, S. Noimark, J. C. Bear, W. J. Peveler, M. Bovis, E. Allan, A. J. MacRobert and I. P. Parkin, *J. Mater. Chem. B*, 2015, **3**, 6490–6500.
31 S. K. Sehmi, S. Noimark, J. Weiner, E. Allan, A. J. MacRobert and I. P. Parkin, *ACS Appl. Mater. Interfaces*, 2015, **7**, 22807–22813.
32 S. Noimark, E. Allan and I. P. Parkin, *Chem. Sci.*, 2014, **5**, 2216–2223.
33 S. Noimark, M. Bovis, A. J. MacRobert, A. Correia, E. Allan, M. Wilson and I. P. Parkin, *RSC Adv.*, 2013, **3**, 18383–18394.
34 N. J. Brown, J. Weiner, M. S. P. Shaffer and C. K. Williams, *Chem. Commun.*, 2013, **49**, 11074.
35 S. D. Pike, E. R. White, M. S. P. Shaffer and C. K. Williams, *Nat. Commun.*, 2016, **7**, 13008.
36 E. Q. Adams and L. Rosenstein, *J. Am. Chem. Soc.*, 2002, **36**, 1452–1473.
37 G. B. Hwang, E. Allan and I. P. Parkin, *ACS Appl. Mater. Interfaces*, 2016, **8**, 15033–15039.
38 E. G. A. Owusu, A. J. MacRobert, I. Naasani, I. P. Parkin, E. Allan and E. Yaghini, *ACS Appl. Mater. Interfaces*, 2019, **11**, 12367–12378.
39 N. Hirota and S. Yamauchi, *J. Photochem. Photobiol., C*, 2003, **4**, 109–124.
40 S. Noimark, E. Salvadori, R. Gómez-Bombarelli, A. J. MacRobert, I. P. Parkin and C. W. M. Kay, *Phys. Chem. Chem. Phys.*, 2016, **18**, 28101–28109.
41 K. J. Heo, S. B. Jeong, J. Shin, G. B. Hwang, H. S. Ko, Y. Kim, D. Y. Choi and J. H. Jung, *Nano Lett.*, 2021, **21**, 1576–1583.
42 G. B. Hwang, H. Huang, G. Wu, J. Shin, A. Kafizas, K. Karu, H. D. Toit, A. M. Alotaibi, L. Mohammad-Hadi, E. Allan, A. J. MacRobert, A. Gavriilidis and I. P. Parkin, *Nat. Commun.*, 2020, **11**, 1207.
43 S. K. Sehmi, C. Lourenco, K. Alkhuder, S. D. Pike, S. Noimark, C. K. Williams, M. S. P. Shaffer, I. P. Parkin, A. J. MacRobert and E. Allan, *ACS Infect. Dis.*, 2020, **6**, 939–946.
44 V. Subramanian, E. E. Wolf and P. V. Kamat, *J. Am. Chem. Soc.*, 2004, **126**, 4943–4950.
45 J. H. Shin, S. B. Jeong, I. H. Kim, S. Y. Lee, G. B. Hwang, I. Park, K. J. Heo and J. H. Jung, *Environ. Res.*, 2023, **238**, 117159.